Electrochemical studies and growth of apatite on Molybdenum doped DLC coatings on titanium alloy β-21S

C. Anandan*, L. Mohan and P. Dilli Babu

Surface Engineering Division, CSIR-National Aerospace Laboratories

P.O.Box:1779, Old Airport Road, Bangalore-560 017

Karnataka, India

Abstract

Titanium alloy β-21S (Ti-15Mo-3Nb-3Al-0.2Si) was coated with molybdenum doped DLC by Plasma-enhanced chemical vapour deposition and sputtering. XRD, XPS and Raman spectroscopy show that Mo is present in the form of carbide in the coating. XPS of samples immersed in Hanks' solution shows presence of calcium, phosphorous and oxygen in hydroxide / phosphate form on the substrate and Mo-doped DLC. Potentiodynamic polarization studies show that the corrosion resistance and passivation behavior of Mo-doped DLC is better than that of substrate. Electrochemical impedance spectroscopy (EIS) studies show that Mo-doped DLC samples behave like an ideal capacitor in Hanks' solution.

Keywords: Titanium alloy, Mo-DLC, apatite growth, corrosion, XPS, EIS.

*Corresponding author email: canandan@nal.res.in.

Phone: 080-25086248 Fax: 080-25210113

1. Introduction

Amongst the materials available for bio-implant applications, the selection of titanium-based materials for implantation is due to their high strength, low density, and high resistance to corrosion, inertness to body environment, enhanced biocompatibility and low modulus [**1**]. The materials used as implants are expected to be highly non toxic and should not cause any inflammatory or allergic reactions in the human body [**2**]. However, titanium-based alloys have a high coefficient of friction that leads to formation of wear debris that results in inflammatory reaction causing pain and loosening of implants due to osteolysis. Further, it has poor shear strength, making it less desirable for bone screws, plates and similar applications [**3**]. Most of the biomedical titanium alloys belong to α + β or metastable β class **[4]**. Since high modulus of α + β titanium alloys results in bone resorption and implant loosening **[5]**, research on many titanium biomaterials is done by focusing on β type titanium alloys, because enhanced properties such as lower modulus of elasticity, increased corrosion resistance, and improved tissue response**.** Therefore, β type titanium alloys composed of non-toxic elements such as Nb, Ta, Zr, Mo, and Sn having lower modulus of elasticity and greater strength should be developed **[6]**. In recent years, Ti–Mo alloys employed as biomaterials have been studied with emphasis on their microstructure, corrosion and mechanical properties **[7, 8]**

Osseointegration which is the process of bone healing and the formation of new bone is the clinical goal of implant surgery. The inability of an implant surface to integrate with the adjacent bone and other tissues due to micro motions results in implant loosening **[9]**. A fibrous tissue is formed between the bone and the implant, if the implant is not well integrated with the bone **[10]**. Hence, materials with an appropriate surface are highly

essential for the implant to integrate well with the adjacent bone. A variety of strategies have been experimented to improve bone integration of titanium-based materials. Surface chemistry, surface roughness and surface topography all play a major role in the development of good osseointegration. The poor tribological and osseointegration properties of the titanium and its alloys lead to the problem of reduced service life of the implants. This problem can be overcome to a large extent by suitable surface coatings. Surface engineering can play a significant role in extending the performance of orthopedic devices made of titanium several times beyond its natural capability **[11]**.

Diamond like Carbon (DLC) is a metastable form of carbon with a significant percentage of sp^3 hybridized carbon. They have high hardness, low coefficient of friction, nontoxic, chemically passive and corrosion resistant. These properties make it ideal for biomedical applications **[12]**. Films with a high proportion of sp^2-bonded carbon atoms tend to be relatively soft and behave more like graphite during tribological tests, while films with more sp^3-bonded carbons are more like diamond and hence they are extremely hard and provide impressive tribological properties. The mechanical properties of DLC depend on the percentage of the different bonding components, C-C (sp^3), C-C (sp^2) and C-H bonds **[13, 14]**. However, a major issue with DLC is its poor adhesion to titanium. Also, the high internal stresses in these coatings make it difficult to obtain coatings thicker than a micron. This problem can be overcome by doping the DLC with a transition metal as they reduce internal stresses thus improving adhesion. For biomedical applications, the dopant metal needs to be also biocompatible. Metals such as Zr, Mo, Ti, and Ta which are known to be biocompatible can be used to dope DLC to improve its adhesion **[15]**. In addition to improving the adhesion, doping may also help in several ways such as improving the

corrosion properties, facilitating cell growth or apatite growth wherever necessary to anchor the implant or impede their growth **[16-20].** The surface chemical behaviour of DLC can be easily tuned by the addition of different elements into the DLC film. The addition of SiO_x to DLC seems to result in a reduction of inflammatory reactions. When Ti-DLC is exposed to a biological environment, the adsorption of different proteins could be altered as a function of the Ti content in the DLC film **[21].** The adsorbed proteins will subsequently influence cell attachment, cell proliferation, and cell differentiation and probably even the tribological behavior **[22]**. However, it has to be ensured that the alloyed DLC is also biocompatible. In the past years a few papers have presented experiments where the biological reactions on DLC have been changed by alloying. Generally, specific chemical composition of the modified films strongly affects the surface energy, and may modify various physical properties and decrease compressive stress, making some metal-doped carbon films suitable for large variety of practical applications **[23, 24]**

Mo-doped DLC coatings were deposited by plasma-enhanced chemical vapor deposition and magnetron sputtering on Ti alloy β-21S (Ti-15Mo-3Nb-3Al-0.2Si) to study its biocompatibility. Micro-Raman, surface hardness, roughness, morphology, wear and corrosion studies were carried out on the coated samples. In the present paper, the electrochemical behavior of the coatings in Hanks' solution and growth of apatite on the Mo-doped DLC is presented. The wear and other properties of the coatings will be presented separately.

2. Experimental Details

2.1 Sample Preparation

Titanium alloy β-21S (Ti-15Mo-3Al-3Nb-0.25Si) (ASTM – grade-21) was cut into samples of 1.5 x 1.5 x 0.2 cm size. The samples were ground by silicon carbide emery papers of different grit sizes to smoothen the surface and then polished to mirror-like finish with 0.03μm alumina powder mixed in distilled water. The polished samples were then ultrasonically cleaned for 15 min in acetone. These samples were then loaded in the vacuum chamber for coating.

2.2 Deposition system

The vacuum chamber was pumped down to a base vacuum of $3x10^{-6}$ mbar by a turbo molecular pump backed with a rotary pump. After reaching the base pressure, the chamber and the gas lines were purged with process gases. The source gases CH_4, Ar, and H_2 were introduced into the chamber by a shower head-type distributer and the flow rates were controlled by MKS make mass flow controllers (MKS Instruments, USA). Process pressure in the chamber was monitored by a MKS make Baratron and controlled by a throttle valve. The plasma was generated by 50 W RF power at a frequency of 13.56 MHz by inductive coupling. Prior to deposition, the samples were etched in hydrogen plasma for 15 min. Mo doped DLC was deposited with a gas mixture of 70% Ar and 30% methane. Mo was sputtered from a 99.95% pure Mo target using a magnetron sputtering gun. The magnetron sputtering gun was powered by a symmetric bi-polar pulsed DC power supply, supplied by MAGPULS Stromversorgungs Systeme GmbH, Germany. Sputter deposition was carried with 300V bias pulse at 10 kHz bias frequency. Substrates were biased with -150V DC

voltage. This resulted in 7.33at% of Mo in the Mo doped DLC coating. A Mo interlayer was deposited for 10 minutes with 100% Ar before Mo doped DLC deposition.

2.3 Immersion and Corrosion studies

Immersion studies were carried out by immersing the substrate and coated samples for 1 day at room temperature in 30 ml of freshly prepared of Simulated Body Fluid, (SBF) namely Hanks' solution with ion concentrations nearly equal to that of human blood plasma (Na^+ =142.0, K^+ =5.0, Mg^{2+} = 1.5, Ca^{2+} = 2.5, HCO_3^- = 4.2, HPO_4^{2-} = 1.0, SO_4^{2-} = 0.50 and Cl^- = 147.96 mM). The chemical composition of the Hanks' solution is as follows: 0.185 g $CaCl_2$, 0.4 g KCl, 0.06 g KH_2PO_4, 0.1 g $MgCl_2 \cdot 6H_2O$, 0.1g $MgSO_4 \cdot 7\ H_2O$, 8.0 g NaCl, 0.35 g $NaHCO_3$, 0.48 g Na_2HPO_4 and 1.00 g d-glucose in 1lit of milli-Q water **[25].** The pH of the solution was adjusted with 1M HCl to 7.2- 7.6 and the experiments were carried out at room temperature.

Electrochemical studies on the substrate and Mo-doped DLC samples were conducted using CHI604D Electrochemical Workstation supplied by CH instruments, USA. The conventional three electrode glass cell was used to carry out the electrochemical studies. The tests were conducted in 200 ml of Hanks' solution which simulates the body fluid (SBF) at room temperature. The sample was kept as the working electrode; Pt foil and saturated calomel electrode (SCE) were used as counter and reference electrodes, respectively. The reference electrode was kept very close to the surface of the working electrode. The sample was immersed in Hanks' solution for an hour in order to establish the open circuit potential (E_{OCP}) or the steady state potential. EIS measurement was carried out in the frequency range of 10 mHz to 100 kHz. The applied alternating sinusoidal potential was 10mV on the E_{OCP}. After

each experiment, the impedance data were displayed as Bode plots. The Bode plot is a plot of log |*Z*| vs. log *f* and log *f* vs. - phase angle (θ), where |*Z*| is the absolute impedance and *f* is the frequency. The acquired data were curve fitted and analyzed using ZSimpwin program (Princeton Applied Research, USA) to get suitable equivalent circuit parameters. The quality of the fit was checked by the χ^2 value. After EIS measurements, potentiodynamic polarization studies were carried out in a potential range of 200 mV below the OCP value to 1000 mV on the positive side with a scan rate of 1mV/s. The measured current–voltage data are plotted as Tafel plots in the form of potential vs. log (i) plot. The corrosion potential (E_{corr}) and corrosion current (I_{corr}) were deduced from the Tafel plot. The corrosion current was obtained using Stern-Geary equation, **[26]**

$$I_{corr} = \frac{\beta_a x \beta_c}{2.3Rp(\beta_a + \beta_{c)}} \quad (1)$$

where, βa and βc are the Tafel slopes of the anodic and cathodic part of Tafel plot and Rp is polarization resistance.

2.4 Characterization techniques

The presence of various phases in the treated sample was identified by X-ray diffraction (XRD) using BRUKER D8 Advance (BRUKER, Germany), X-ray diffractometer. Monochromatic Cu Kα radiation (λ = 0.1548 nm) was used and the samples were scanned from 30° to 70° at a scanning rate of 0.02°/min. Micro Raman studies were performed with DILOR-JOBIN-SPEX made LABRAM 010, France. A He-Ne laser source having a wavelength of 632 nm was used. XPS spectra were obtained in a SPECS XPS system (M/s.

SPECS Surface Nano Analysis GmbH, Germany) equipped with a twin anode X-ray source and a hemispherical analyzer with single channel detector. The spectra were obtained with 150W non-monochromatic Al Kα radiation (1486.6eV). Core level spectra of O1s, C1s, Ti2p, Mo3d, Ca2p and P2p were obtained at a pass energy of 25eV. O1s, C1s and Mo3d core level spectra were fitted with Gaussian-Lorentzian peaks to identify various species after subtracting a Shirley-type background.

3. Results and discussion

X-ray diffraction patterns from the substrate and Mo doped DLC samples are given in **Fig. 1.** The inset in the figure shows the diffraction patterns in the $38^{\circ} - 40^{\circ}$ 2θ range. The location of different peaks pertaining to beta (β) phase, MoC and Mo_2C are shown in the figure. The substrate pattern (a) shows two dominant peaks due to bcc phase. After depositing Mo doped DLC, in diffractogram (b) broad peak corresponding to MoC at 39.1° (JCPDS #89-4305) and Mo_2C at 39.4° (JCPDS #71-0242) are present. In the inset, the separation of β and molybdenum carbides is clear in the 38° to 39.5° range in diffractogram (b) for the Mo doped DLC. These features suggest the presence of molybdenum carbides **[27]**.

The micro Raman spectrum of pure DLC is compared with that of Mo-doped DLC coatings in 1000–1800 cm^{-1} wave number range in **Fig.2 (a** and **b).** The spectra were fitted with Gaussian peaks to estimate the sp^3/sp^2 ratio. Usually, the Raman spectra of DLC films are characterized by a G peak around 1550 cm^{-1} and a D shoulder around 1350 cm^{-1}. The G peak is due to the bond stretching of all pairs of sp^2 atoms in both rings and chains, and the D peak is due to the breathing modes of sp^2 atoms in rings. However, it has been suggested that a good fit of the Raman spectra of DLC needs four Gaussian peaks **[28, 29]**. The peaks around

1200 and 1500 cm^{-1} correspond to the sum and difference of the C=C chain stretching and C-H wagging modes of trans polyacetylene and the other resonating double bond **[30-32]**. In this study, the Raman spectra of pure DLC and Mo-doped DLC were fitted with four peaks and the ratio of D peak at 1360 cm^{-1} to the G peak at 1550 cm^{-1} is used to estimate the sp^3/sp^2 ratio **[33, 34]**. The sp^3/sp^2 values represent the degree of disorder in the carbon network. The sp^3/sp^2 ratio of pure DLC is 1.3 and for Mo doped DLC coatings is 1.8. Thus incorporation of Mo in DLC increases the disorder. **Fig. 2(c)** shows the Raman spectra in the 100–1100 cm^{-1} wave number range of the Mo-doped DLC samples. Peaks at 285, 335, 376, 470, 666, 819 and 995 cm^{-1} can be seen which correspond to that of molybdenum carbide [**35**]. This shows that molybdenum doping has resulted in the formation of molybdenum carbide in the coating.

Figs. 3(a) and (b), shows the carbon 1s spectra of the Mo doped DLC samples in the as-received condition and after 1 day immersion in SBF. The spectra were fitted with four Gaussian-Lorentzian components to identify the various bonding schemes of carbon. The ratio of sp^3/sp^2 carbon atoms is one of the most important factors governing the quality of the DLC films **[36]**. In the spectra, binding energies of the peaks at 284.3 eV and 285.8 eV correspond to the C- C (sp^2) and C- C (sp^3) forms, respectively. A peak of smaller intensity at 286.9 eV has also been added and is attributed to some C–O contamination formed at the surface of the samples due to air exposure and immersion in SBF. The peak at 282.8 eV shows carbon in metallic carbide form due to the formation of carbides of Mo. The percentage of carbon presents as C- C (sp^2), C- C (sp^3), Mo-C and C-O is given in **Table 1**. The peak positions of the species marked in **Figs. 3 (a)** and (**b)** are given in **Table 2.** The

table and figures show the higher sp^3 content and formation of MoC in Mo doped DLC samples, which is further substantiated by micro Raman and XRD respectively.

Fig. 4 (a) and **(b)** show the Ti2p core level spectra from the substrate as received and after one day immersion in SBF respectively. In **Fig. 4(a)**, the Ti2p spectrum for the substrate shows presence of metallic Ti at 454.1eV binding energy (BE) and titanium in TiO_2 state as evidenced from a binding energy of 458.9eV for the $Ti2p_{3/2}$ component. After one day immersion in Hanks' solution, the substrate surface is completely covered with TiO_2 as in **Fig.4 (b)** has no trace of Ti metallic peak. This shows that the surface is completely covered by oxide after 1day immersion in SBF. After Mo-doped DLC coating, no trace of Ti related signals were detected as the substrate surface is completely covered with Mo doped DLC.

Figs. 5(a) and **(c)** show the Mo3d core level spectra from the substrate and Mo doped DLC coated samples, respectively, in the as received condition. The spectra were fitted with Gaussian-Lorentzian components to identify the various components of Mo. Curve-fitting of Mo 3d peaks was accomplished using linked doublets (Mo $3d_{5/2}$ – Mo $3d_{3/2}$) corresponding to three different molybdenum species (Mo^0, Mo^{+4} and Mo^{+6}) on substrate and four species (MoC, Mo_2C, Mo^{+4} and Mo^{+6}) on Mo doped DLC samples. **Table 2** lists the binding energies of Mo3d core level in different compounds. According to the literature, **[37]** the peaks found at 227.7 eV and 227.8 eV can be attributed to Mo^0 state, and carbide phase of Mo for Mo_2C respectively **[38].** Similarly the binding energy found around 228.8 eV can be attributed to a carbide phase of Mo in MoC **[39]**. Molybdenum in MoO_2 and MoO_3 oxidation states has binding energies of 229.0 and 232.6 eV, respectively. The at% of various components of

Mo3d such as Mo^0, Mo^{+4} and Mo^{+6} for substrate and MoC, Mo_2C, Mo^{+4} and Mo^{+6} for Mo doped DLC samples in as-received and after one day immersion in SBF are given in the **Table 3**. On the substrate surface, the molybdenum $3d_{5/2}$, **Fig. 5(a),** peaks can be identified at 227.7 eV for metallic Mo, 229.0 eV for molybdenum in Mo^{+4} form and at 232.6eV for molybdenum in Mo^{+6}. After Mo doped DLC deposition the carbide peaks at 227.8 and 228.8 eV can be seen in **Fig. 5(c).** This shows the presence of molybdenum carbide in Mo doped DLC coating which corroborates the XRD results. **Figs. 5(b)** and **(d)** show the Mo3d core level spectra from the substrate and Mo doped DLC coated samples after one day immersion in SBF, respectively. As can be seen in **Fig. 5(b)** and **Table 3**, the percentage of the metallic peak of Mo (Mo^0) in substrate has decreased and molybdenum is mostly present as MoO_3, in the 6+ state after one day immersion in SBF. As can be seen in **Fig. 5(d)** and **Table 3**, the percentage of the carbide peaks of Mo (MoC and Mo_2C) and Mo^{+6} in Mo-doped DLC has decreased with increased Mo^{+4} concentrations and molybdenum is mostly present as MoO_2, in the 4+ state after one day immersion in Hank's solution.

Figs.6 (a) and **(b)** shows XPS spectra of Ca2p and P2p core level from the substrate and Mo doped DLC samples in the as-received condition and after 1 day immersion in SBF. In these spectra, intensities of Ca2p and P2p peaks at 347.3eV and 133.6eV binding energies, respectively, confirm the formation of calcium phosphate (CP) phases on the substrate and Mo doped DLC. As can be seen in **Fig. 6**, and **Table 4** the relative intensities of Ca and P is more on the Mo doped DLC in comparison to the substrate. As Mo is a known biomaterial, Mo incorporation into the DLC coating induces formation of CP phases. The stable phases of

calcium phosphate depend considerably upon temperature and the presence of water, either during processing or in the environment. The formation of the CP phases interact with water or body fluids to form hydroxyapatite [Ca_{10} $(PO_4)_6$ $(OH)_2$], HAP the principal component of bone material **[40].**

Figs. 7 (a) and **(b)** show the oxygen 1s core level spectra from the substrate and Mo-doped DLC samples after 1day immersion in SBF. The spectra were fitted with three Gaussian-Lorentzian components to identify the various bonding schemes of oxygen. The O1s core level BE in metal oxide (O^{2-}), OH^-/phosphate ion (PO_4^{3-}) and in adsorbed water are at 530.0, 531.4 and 533.4 eV, respectively **[41-45].** The peak positions of the species are marked in **Figs. 7** (**a)** and (**b).** The percentage of oxygen present as O^{2-}, OH^-/ (PO_4^{3-}) and in water molecule is given in **Table 5**. The presence of OH^-/ (PO_4^{3-}) related peak shows that hydroxyapatite, i.e. hydrated calcium phosphate may be present on the surface. It can be seen from the figure that in the case of substrate the metal oxide component (O^{2-}) is 63.3 at% and OH^- component is 30.3% in the as-received condition. After 1day immersion, the OH^-/ (PO_4^{3-}) component has increased to 42.8%. In the case of Mo-doped DLC samples, the metal oxide component (O^{2-}) is 24.5% and OH^- component is 58.1% in the as-received condition. After 1day immersion, the oxide component has decreased to about 10%, adsorbed water molecule was 25.2% and the OH^-/ PO_4^{3-} has increased to 64.7%. Thus, Mo –doped DLC has more oxygen in the form of OH^-/ (PO_4^{3-}) species or water molecule in SBF environment than substrate. Apatite, the bone constituent is generally present as hydroxyapatite. Therefore, the higher OH^-/ (PO_4^{3-}) adsorbing property of Mo doped DLC is advantageous for biomedical implant applications. Therefore, Mo in Mo doped DLC is able to form hydroxide and adsorb water molecules as evidenced from the O1s spectra in **Fig.7**.

Potentiodynamic polarization curves of the substrate and Mo doped DLC coated substrates in SBF (Hanks' solution) are shown in **Fig. 8.** The corrosion current (I_{corr}) was obtained by extrapolation of the anodic and cathodic branches of the polarization curves to the corrosion potential using the equation (1). **Table 6** shows the corrosion current density, corrosion potential and polarization resistance for the substrate and Mo doped DLC coated substrate. The corrosion current density, (I_{corr}) is 0.076μA/cm^2 for the substrate and 0.012 μA/cm^2 for the Mo doped DLC coated substrate. Thus, coating has increased the substrate's corrosion resistance. It can be also seen from **Fig. 8** that the current for formation of a passive film is slightly lower for Mo doped DLC coated samples and the current remains lower than that of substrate up to 1V. This shows that the Mo doped DLC has better passivation properties compared to that of the substrate. The E_{corr} value shifted to much nobler value, -0.118 V for Mo doped DLC sample, compared to the substrate value of -0.290V. The values of polarization resistance given in **Table 6** shows that Mo-doped DLC possess good resistance for corrosion.

The results of electrochemical impedance test in Hanks' solution are presented in **Fig. 9** in the form of Bode plot. The limiting impedance at the high frequency end corresponds to solution resistance, R_e. In **Fig. 9 (a)**, for substrate, the phase angle changes rapidly from -0^o to -20^o in the high frequency range (10 to 100 kHz). In the low frequency range from 0.01Hz to 100 Hz, the phase angle remains nearly constant and less than -90^o (-82^o), the value for an ideal capacitor. In the same frequency range, a linear relationship between log |*z*| and log *f* is observed with a slope close to one. In the case of Mo doped DLC sample **Fig. 9 (b)**, the phase angle in the frequency range of 0.1Hz to 10Hz is -84.5^o and decreases to -73^o in the lower frequency range.

Fig. 10 (a) and **(b)** show the equivalent circuit models used for fitting the EIS data of the substrate and Mo doped DLC coated samples, respectively. The equivalent electrochemical circuit is composed of resistances and constant phase elements (CPE). The resistive components Re, R1 and R2 are related to the solution resistance, outer layer resistance and inner layer resistance, respectively. The Q symbol signifies the possibility of a non-ideal capacitance, known as constant phase element (CPE), whose impedance is defined as $Z_{CPE} = [Q (j\omega n)]^{-1}$ with 'n' less than 1; for an ideal capacitance n = 1. In this, Q1 represents the capacitance of the outer layer, Q2 the capacitance of the inner layer. The fitted curves are also shown in **Fig. 9 (a).** Previous researchers have proposed a circuit model similar to that in **Fig10 (a)** to simulate the EIS data of oxide films on Ti alloy in various solutions that simulate body fluids. **[46, 47].** Similar equivalent circuits have been also proposed for beta titanium alloys in aqueous chloride and Hanks' solutions **[48-52].** The equivalent circuit used for fitting the impedance data of Mo doped DLC sample is shown in **Fig. 10(b).** In this system, the inner layer is represented by the elements Q2 and R2 that correspond to CPE and resistance of inner Mo doped DLC coating. Q1 and R1 represent the CPE and charge transfer resistance of the outer layer. This layer acts in parallel with inner layer.

The values of the electrical parameters obtained by fitting the impedance data of the substrate and Mo doped DLC samples are given in **Table 7.** For the substrate, the high corrosion resistance R2 is associated with inner oxide layer on the substrate, which is 1.58×10^7 Ωcm^2 in the present case. The Q2 component is associated to the capacitance of this inner barrier layer. The resistance of outer porous layer is 19.4 Ωcm^2. The value "n" for the constant phase element representing the outer layer is 0.90 and that representing the inner layer is 0.91. The results for Mo doped DLC coated samples in **Table 7** show that the resistance R1

of the outer layer is about 22 Ωcm^2 and that of the inner Mo doped DLC layer (R2) is about 2.50 $x10^6$ Ωcm^2. The non ideal value for the constant phase element representing the outer layer is 0.90 and that representing the inner layer is 0.92. There is deviation from near ideal capacitor behavior in very low frequency range (0.1 to 0.01 Hz) as the phase angle is ~ -70^o. The high R2 value (**Table 7**) of the Mo doped DLC film shows that the Mo doped DLC layer possess good corrosion resistance. The barrier layer (Mo doped DLC layer) resistance of coated samples is one order lower compared to that of substrate one. This could be due to doping of DLC with metal. However, the polarization resistance of the Mo doped DLC is higher than that of substrate with better passivation behavior in simulated body fluid environment. Also, Mo doping helps in formation of CP phases which leading to hydroxyapatite, the principle component of bone material. In addition to the above, it is well known that doping of DLC with metals improves its adhesion to titanium alloys and also improve their tribological properties. Therefore, Mo doped DLC can be further investigated as a biocompatible coating on titanium alloys.

Conclusions

Mo-doped DLC has been deposited on β-21S (Ti-15Mo-3Nb-3Al-0.2Si) biomedical titanium alloy by PECVD and magnetron sputtering. XPS results clearly demonstrated the distribution of Mo oxidation states on substrate and Mo-doped DLC samples before and after immersion in SBF. As evidenced from surface sensitive XPS studies formation of (CP) calcium phosphate phases on Mo-doped DLC samples is higher compared to that of substrate after one day immersion in SBF. Potentiodynamic polarization and electrochemical impedance

studies in Hanks' solution show that Mo-doped DLC has good corrosion resistance with better passivation behavior. Hence, doping of Mo with DLC helps in formation of CP phases which leading to hydroxyapatite, the principle component of bone material and better corrosion resistance properties.

Acknowledgments:

The authors would like to thank the Director, National Aerospace Laboratories, Bangalore for his support and permission to publish the work. The authors would like to thank Mr. Srinivas and Mr. N.T. Manikandanath for XRD and Micro Raman studies.

References

[1] Yoshiki Oshida, Bioscience and bio engineering of Titanium Materials, first ed., Elsevier, UK, Amsterdam, The Netherlands, 2007.

[2] X. Liu, P. K. Chu, C. Ding, Mater. Sci. Eng. R: Rep., 47 (2004) 49.

[3] B. D. Ratner, A. S. Hoffman, Biomaterials Science; An Introduction to Materials in Medicine, Academic Press, USA, 1996.

[4] G.Lutjering, J.C.Williams, Titanium, Engineering Materials and Processes, second ed., Springer,Verlag Berlin Heidelberg, 2007, pp. 283-332.

[5] S. Sathish, M. Geetha, N.D. Pandey, C. Richard, R. Asokamani, Mater. Sci. Eng. C 30 (2010) 376.

[6] M. Niinomi, D. Kuroda, K. Fukunaga, M. Morinaga, Y. Kato, T. Yashiro, et a*l*. Mater. Sci. Eng. A 263 (1999)193.

[7] N.T.C. Oliveira, G. Aleixo, R. Caram, A.C. Guastaldi, J. Mater. Sci. Eng. A 452-453 (2007) 727.

[8] N.T.C. Oliveira, A.C. Guastaldi, Acta Biomater. 5 (2009) 399.

[9] M. Viceconti, R. Muccini, M. Bernakiewicz, M. Baleani, L. J. Cristofolini, Biomech. 33(2000)1611.

[10] L. Mohan, D. Durgalakshmi, M. Geetha, T. S. N. Sankaranarayanan, R. Asokamani, Ceram. Inter. 38 **(**2012) 3435.

[11] M.Geetha, A. K. Singh, R. Asokamani, A. K. Gogia, Prog. Mater. Sci. 54 (2009) 397.

[12] R. Hauert, Diamond Relat. Mater. 12 (2003) 583.

[13] A. Grill, Surf. Coat. Technol. 94-95 (1997) 507.

[14] A.C. Ferrari, Diamond Relat. Mater. 11 (2002) 1053.

[15] L. Mohan, P. Dilli Babu, Prateek Kumar, C. Anandan, Surf. Interface Anal. DOI 10.1002/sia.5323

[16] Y. Chang, Thin Solid Films 420-421 (2002) 241.

[17] C. Donnet, Surf.Coat. Technol. 100–101 (1998) 180.

[18] Y. Liu, E.I. Meletis, Surf. Coat. Technol. 153 (2002) 178.

[19] Y.F. Zheng, X.L. Liu, H.F. Zhang, Surf. Coat. Technol. 202 (2008) 3011.

[20] G.F. Yin, J.M. Luo, C.Q. Zheng, H.H. Tong, Y.F. Huo, L.L. Mu, Thin Solid Films, 345 (1999) 67.

[21] R. Hauert, L. Knoblauch-Meyer, G. Francz, A. Schroeder, E. Wintermantel, Surf. Coat. Technol. 120–121(1999) 291.

[22] A. Schroeder, G. Francz, A. Bruinink, R. Hauert, J. Mayer, E. Wintermantel, Biomater. 21(2000) 449.

[23] P. A. Dearnley, Proceedings of the Institution of Mechanical Engineers. Part H. J. Eng. Med. 213 (1999) 107.

[24] R. Hauert, Tribology of Diamond-Like Carbon Films: Fundamentals and Applications, DLC Films in Biomedical Applications, Springer, New York, USA, 2008, pp.494.

[25] C. Anandan, L. Mohan, J. Mater. Eng. Perform. DOI: 10.1007/s11665-013-0628-6

[26] M. Stern, A. L. Geary, J. Electrochem. Soc. 104 (1957) 56.

[27] Li Ji, H.Li, F. Zhao, J. Chen, H. Diamond Relat. Mater. 17 (2008) 1949.

[28] F.C. Tai, S.C. Lee, J. Chen, C. Wei, S.H. Chang, J. Raman Spectrosc. 40 (2009) 1055.

[29] A. Ferrari, J. Robertson, Diamond, Phys. Rev. B 63 (2001) 2.

[30] A.C. Ferrari, J. Robertson, Phys. Rev. B 61 (2000) 95.

[31] A.C. Ferrari, Mater. Res. 675 (2001) 1.

[32] G. Irmer, A. Dorner-Reisel, Adv. Eng. Mater. 7 (2005) 694.

[33] F.X. Liu, K.-L. Yao, Z.-L. Liu, J. Non-Cryst. Solids 353 (2007) 2545.

[34] Prateek Kumar, P. Dilli Babu, L. Mohan, C. Anandan, V.K. William Grips, J. Mater. Eng. Perform. 22 (2013) 283.

[35] M.L.Frauwallner, F. L. Linares, J. L.Romero, C.E. Scott, V. Ali, E. Hernández, P.P.Almao, Appl. Catal. A: Gen. 394 (2011) 62.

[36] P. Merel, M. Tabbal, M. Chaker, S. Moisa, J. Margot, Appl. Surf. Sci. 136 (1998) 105.

[37] W.A Brainard, D.R. Wheeler, J. Vac. Sci. Technol. 15 (1978) 1801.

[38] J.M. Manoli, P. Da Costa, M. Brun, M. Vrinat, F. Mauge, C. Potvin, J. Catal. 221 (2004) 365.

[39] M. Xiang, D.Li, J.Zou1, W. Li, Y.Sun, X. She, J. Nat. Gas Chem. 19 (2010)151.

[40] C. C. Chusuei, D. W.Goodman, Anal. Chem. 71 (1999) 149.

[41] C.O.A. Olsson, D. Landolt, Corros. Sci. 46 (2004) 213.

[42] De Sena LA, N.C.C. Rocha, M.C. Andrade, G.A. Soares, Surf. Coat. Technol. 166 (2003) 254.

[43] V. Maurice, G. Despert, S. Zanna, P. Josso, M.P. Bacos, P. Marcus, Acta Mater. 55 (2007) 3315.

[44] E. McCafferty, J.P. Wightman, Appl. Surf. Sci. 143 (1999) 92.

[45] L. Mohan, C. Anandan, Appl. Surf. Sci. 282 (2013) 281.

[46] S.L. Assis, S. Wolynec, I. Costa, Mater. Corros. 59 (2008) 739.

[47] S.L. Assis, I. Costa, Mater. Corros. 58 (2007) 329.

[48] D.G. Kolman, J.R. Scully, J. Electrochem. Soc. 140 (1993) 2771.

[49] D.G Kolman, J.R. Scully, J. Electrochem. Soc. 14 (1994) 2633.

[50] L. Mohan, C. Anandan, Appl. Surf. Sci. 268 (2013) 288.

[51] L. Mohan, C. Anandan, V.K. William Grips, Appl. Surf. Sci. 258 (2012) 6331.

[52] L. Mohan, C. Anandan, V.K. William Grips, J. Mater. Sci: Mater. Med. 24 (2013) 623.

Table 1 At% of carbon bonded as Mo-C, sp^2, sp^3 and C-O

	Mo-doped DLC	
	As received	**After 1 day immersion**
Species	**at%**	**at%**
Mo-C	06.1	05.3
sp^2	37.4	36.7
sp^3	43.3	38.3
C-O	13.2	19.7

Table 2 Binding energy of Mo3d and C1s core levels in different compounds.

Species	*BE (eV)	
	$Mo3d_{5/2}$	$Mo3d_{3/2}$
Mo^0	227.7	230.8
Mo_2C	227.8	230.7
MoC	228.8	231.8
MoO_2	229.0	232.2
MoO_3	232.6	235.8
	C1s	
C1s(carbide)	282.7	
C-C (sp^2)	284.3	
C-C (sp^3)	285.8	

* http://srdata.nist.gov/xps/

Table 3 Distribution of Mo oxidation states of substrate and Mo doped DLC samples as determined by XPS

		Distribution of Mo oxidation states at %				
		Mo^{0}	**Mo_2C**	**MoC**	**Mo^{+4}**	**Mo^{+6}**
Substrate	**As-received**	46.0	-	-	40.0	13.9
	After immersion	2.2	-	-	47.2	50.6
Mo doped DLC	**As-received**	-	8.3	18.6	39.8	24.1
	After immersion	-	5.9	16.3	62.9	15.2

Table 4 Relative intensities of Ca2p and P2p from core level XPS spectra of substrate and Mo-doped DLC samples after 1day immersion in SBF

	Relative intensity (%)	
	Ca2p	**P2p**
Substrate	16.5	31.7
Mo-doped DLC	83.5	68.3

Table 5 At% of Oxygen bonded as metal oxide O^{2-}, OH^- (or) PO_4^{3-}, and H_2O

Species	Substrate		Mo-doped DLC	
	As received	After 1 day immersion	As received	After 1 day immersion
	At%	At%	At%	At%
O^{2-}	63.3	48.8	24.5	10.1
OH^- (or) PO_4^{3-}	30.3	42.8	58.1	64.7
H_2O	06.4	08.4	17.4	25.2

Table 6 Results of potentiodynamic polarization studies.

S. no	Sample	E_{corr} (V)	i_{corr} (μA/cm^2)	R_P (Ω cm^2)
1.	Substrate	-0.290	0.076	2.6 x 10^6
2.	Mo-doped DLC	-0.118	0.012	1.4 x 10^6

Table 7 Electrochemical impedance parameters obtained by fitting equivalent circuit model for substrate and Mo-doped DLC samples.

Samples	$\mathbf{R_e}$ ($\mathbf{\Omega\ cm^2}$)	$\mathbf{Q_1}$ $\mathbf{S\ s^n\ cm^{-2}}$	$\mathbf{n_1}$	$\mathbf{R_1}$ ($\mathbf{\Omega\ cm^2}$)	$\mathbf{Q_2}$ $\mathbf{S\ s^n\ cm^{-2}}$	$\mathbf{n_2}$	$\mathbf{R_2}$ ($\mathbf{\Omega\ cm^2}$)	$\mathbf{\chi^2}$
Substrate	17.4	3.81×10^{-7}	0.90	19.4	2.57×10^{-5}	0.91	1.58×10^{7}	8.22×10^{-4}
Mo-doped DLC	15.4	2.86×10^{-7}	0.90	22.1	1.11×10^{-5}	0.92	2.50×10^{6}	5.61×10^{-4}

Figure Captions

Fig.1. X-ray diffraction pattern for **(a)** substrate, **(b)** Mo-doped DLC. Inset shows the XRD for the same in the 38 to 40^{o} 2θ range

Fig. 2. Raman spectra of (a) pure DLC (b) and (c) Mo-doped DLC coated samples

Fig.3. XPS spectra of C1s core level along with the fitted curves of Mo-doped DLC (a) as-received and (b) after 1 day immersion in SBF

Fig. 4. XPS spectra of Ti2p core level from substrate **(a)** as-received and **(b)** after 1day immersion in SBF.

Fig.5. XPS spectra of Mo3d core level along with the fitted curves of substrate (a) as-received, and (b) after 1 day immersion in SBF and Mo-doped DLC (c) as-received and (d) after 1 day immersion in SBF

Fig.6. XPS spectra of (a) **Ca2p** and (b) **P2p** core level from substrate and Mo-doped DLC samples after 1day immersion in SBF.

Fig.7. XPS spectra of **O1s** core level from substrate **(a)** and Mo-doped DLC samples **(b); (1)** as-received, **(2)** after 1day immersion in SBF

Fig. 8. Potentiodynamic polarization curves for **(a)** substrate; **(b)** Mo-doped DLC samples.

Fig. 9. Bode plots obtained in Hanks' solution for: (a) substrate; (b) Mo-doped DLC samples; ◆ |Z| measured; ■ |Z| calculated; ▲ angle measured; ◊ angle calculated.

Fig.10. Equivalent circuit diagrams used for fitting EIS data of **(a)** substrate and **(b)** Mo-doped DLC samples.

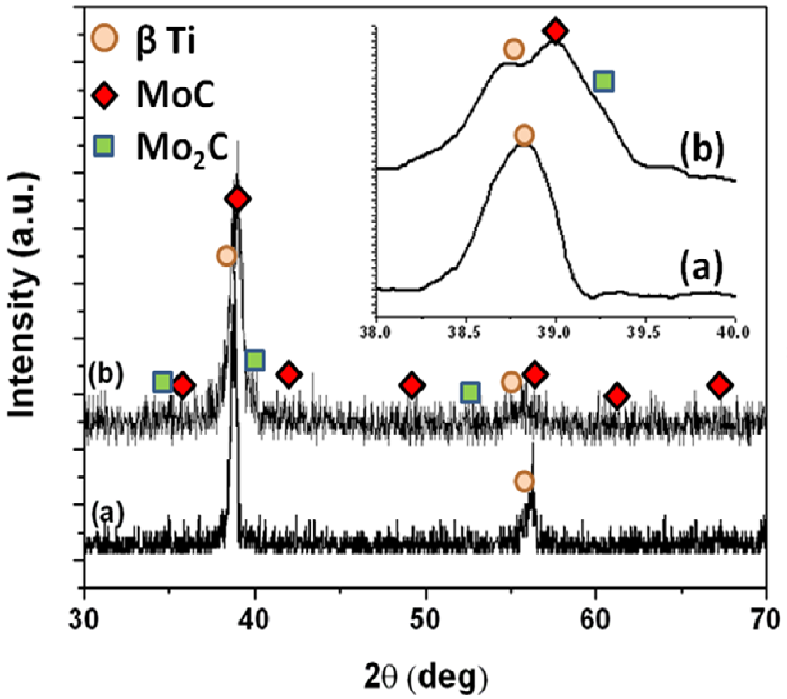

Fig.1. X-ray diffraction pattern for **(a)** substrate, **(b)** Mo-doped DLC. Inset shows the XRD for the same in the 38 to 40^{o} 2θ range

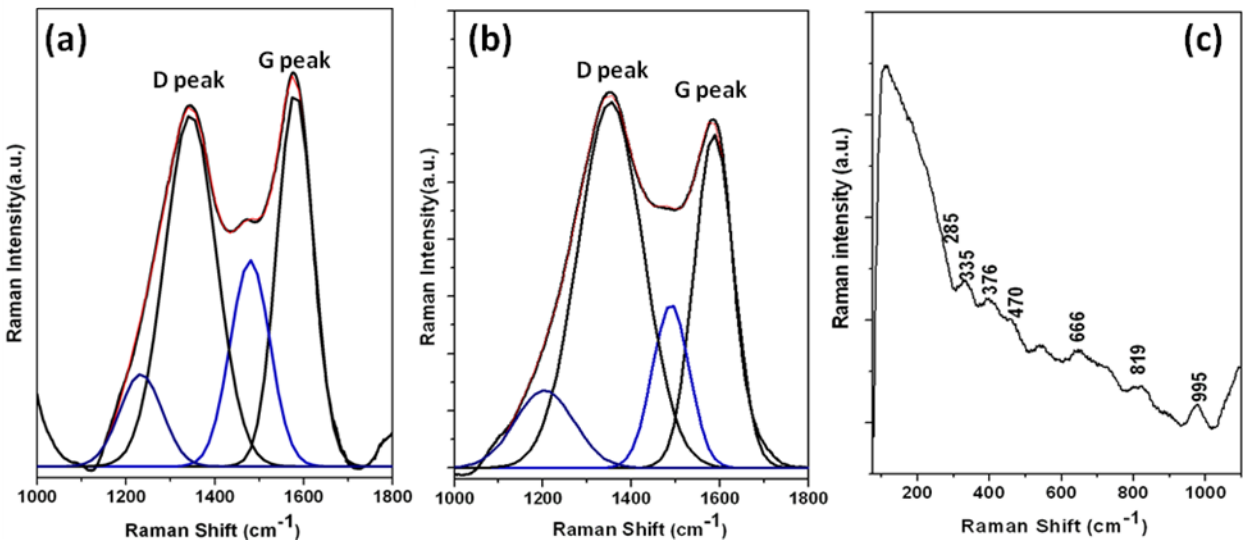

Fig. 2. Raman spectra of (a) pure DLC (b) and (c) Mo-doped DLC coated samples

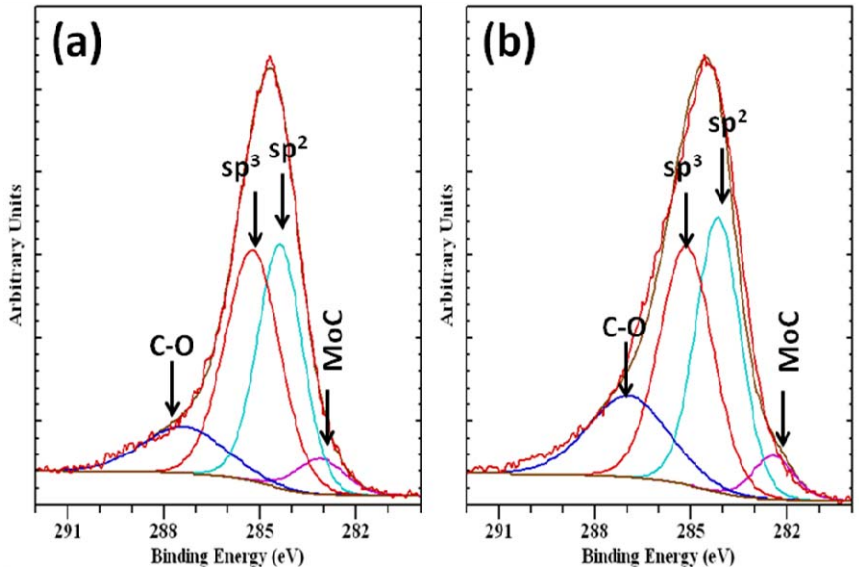

Fig.3. XPS spectra of C1s core level along with the fitted curves of Mo-doped DLC (a) as-received and (b) after 1 day immersion in SBF

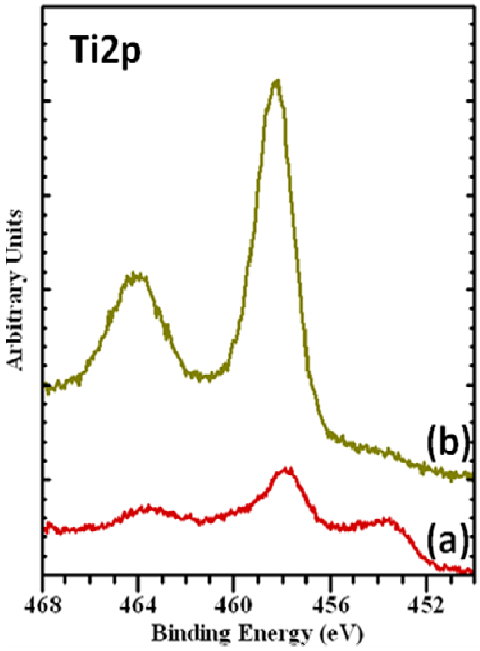

Fig. 4. XPS spectra of Ti2p core level from substrate **(a)** as-received and **(b)** after 1day immersion in SBF.

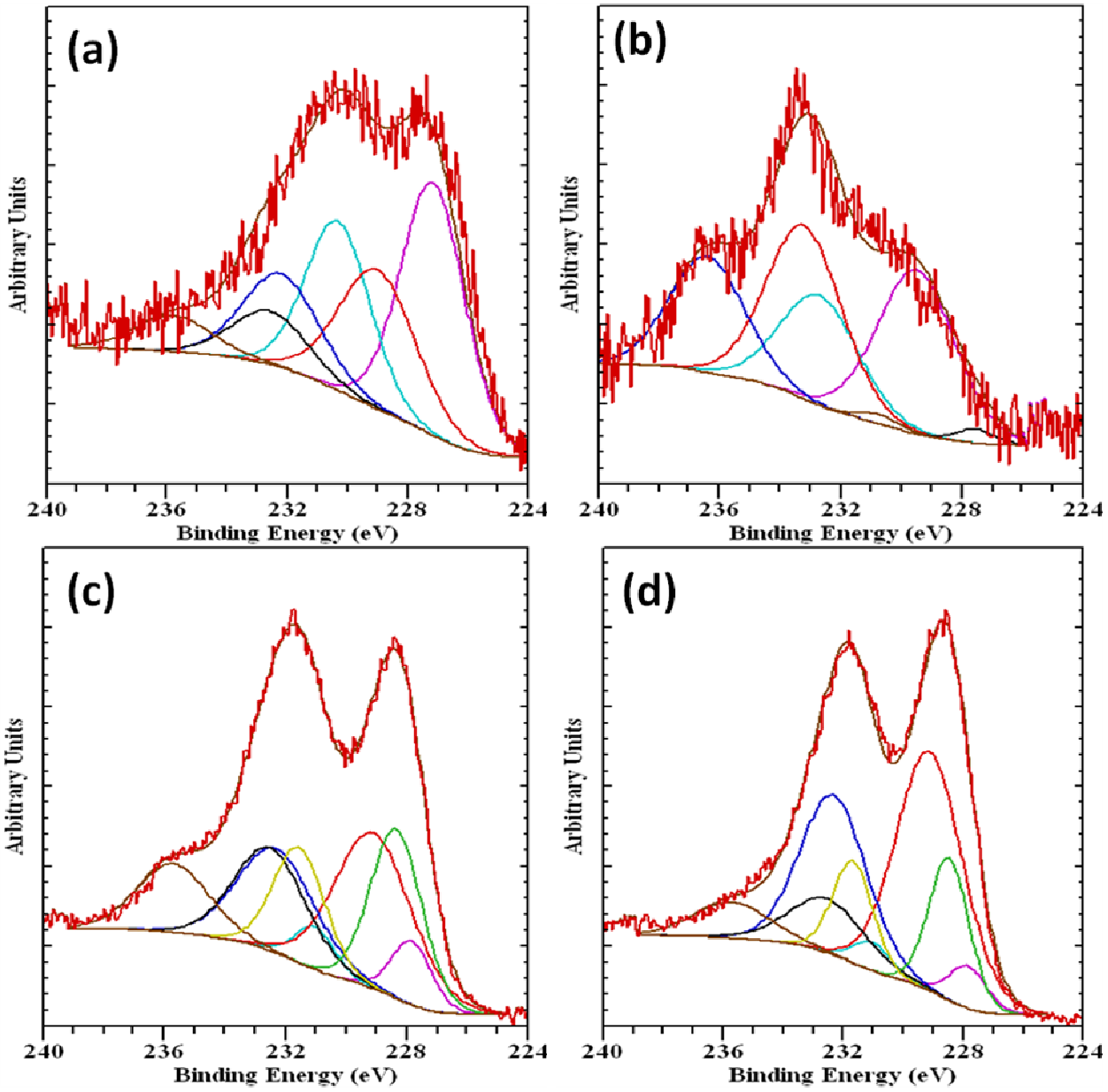

Fig.5. XPS spectra of Mo3d core level along with the fitted curves of substrate (a) as-received, and (b) after 1 day immersion in SBF and Mo-doped DLC (c) as-received and (d) after 1 day immersion in SBF

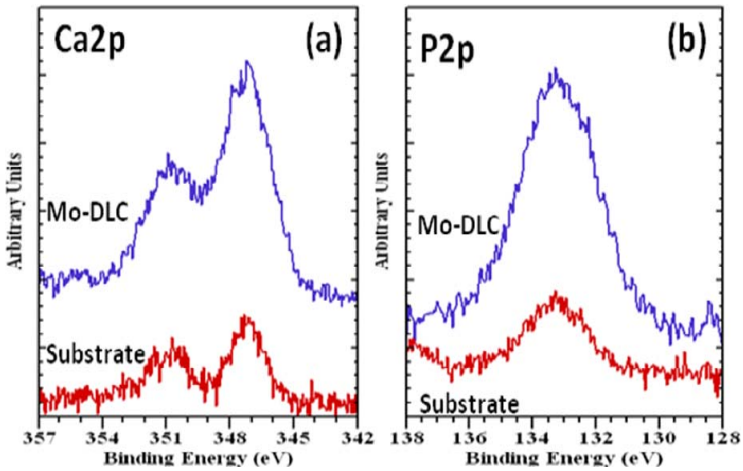

Fig.6. XPS spectra of (a) **Ca2p** and (b) **P2p** core level from substrate and Mo-doped DLC samples after 1day immersion in SBF.

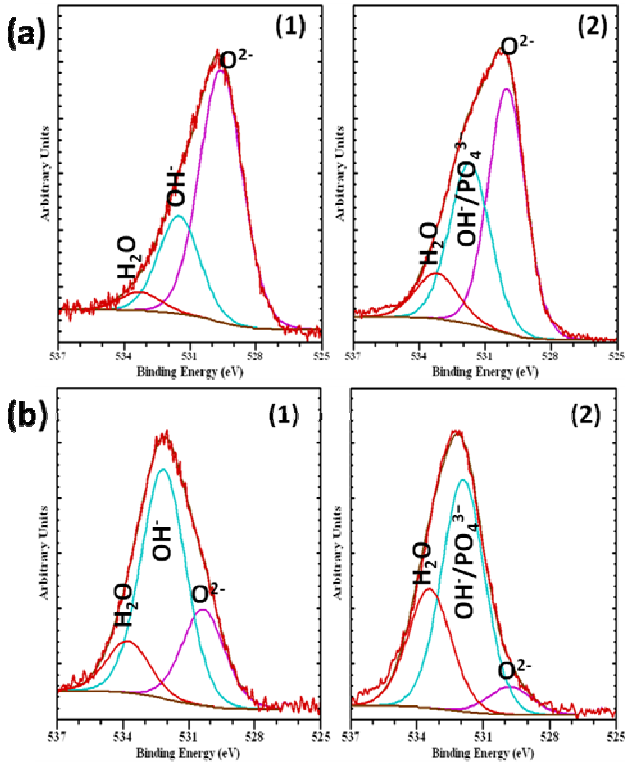

Fig.7. XPS spectra of **O1s** core level from substrate **(a)** and Mo-doped DLC samples **(b); (1)** as-received, **(2)** after 1day immersion in SBF

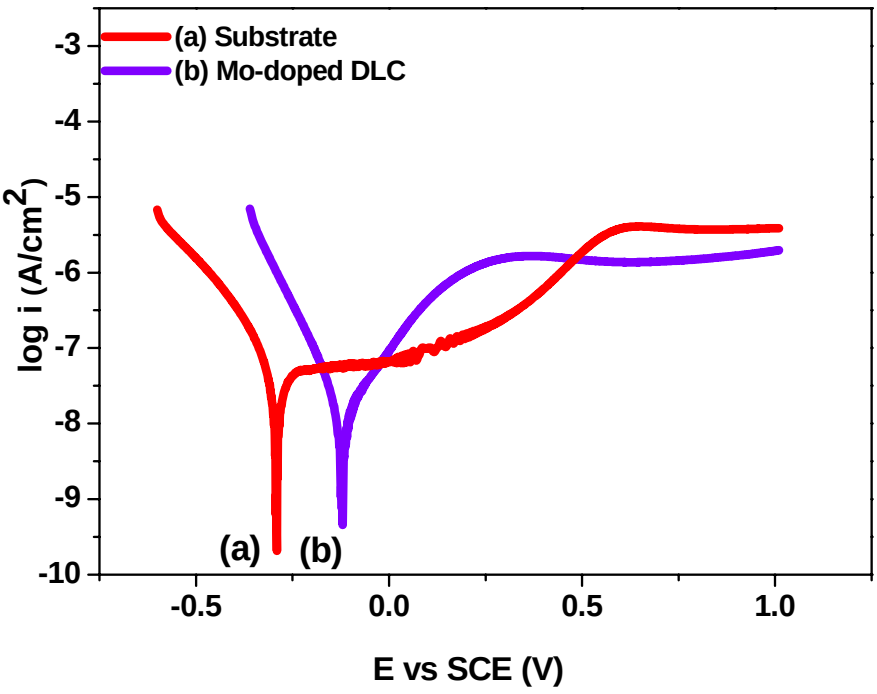

Fig. 8. Potentiodynamic polarization curves for **(a)** substrate; **(b)** Mo-doped DLC samples.

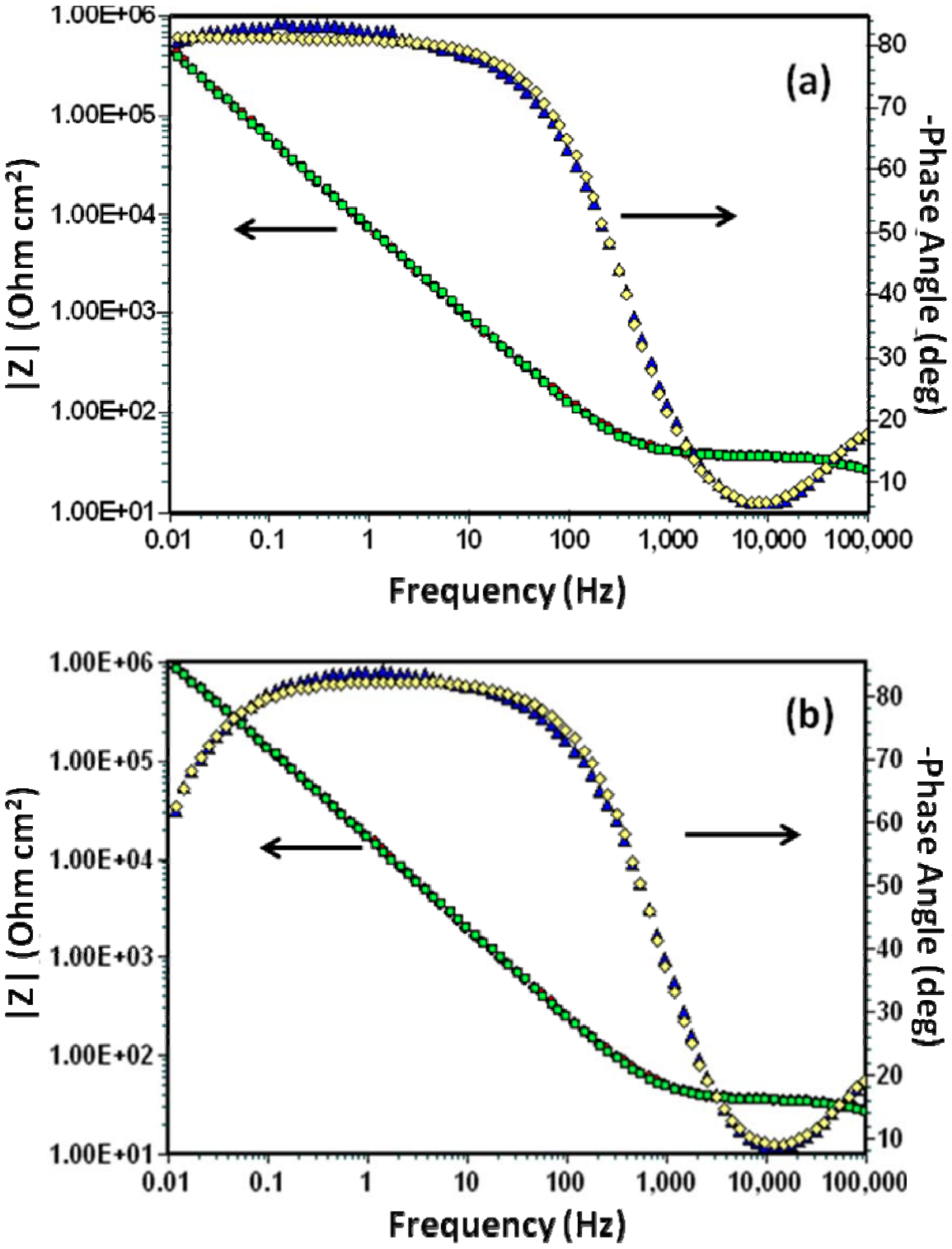

Fig. 9. Bode plots obtained in Hanks' solution for: (a) substrate; (b) Mo-doped DLC samples; ◆ |Z| measured; ■ |Z| calculated; ▲ angle measured; ◊ angle calculated.

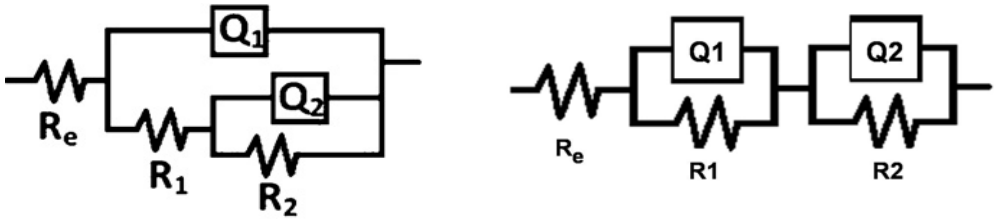

(a) **(b)**

Fig.10. Equivalent circuit diagrams used for fitting EIS data of **(a)** substrate and **(b)** Mo-doped DLC samples.